

Article

Natural Light Rechargeable Night Peal-like Coatings for Expressway

Xin Li ¹, Rong Chen ¹, Rui Xiao ¹, Wenjie Li ¹, Te Si ¹, Peiyang Li ²  and Qi Zhu ^{2,*}

¹ Sichuan Transportation Construction Group Co., Ltd., Chengdu 610041, China

² Key Laboratory for Anisotropy and Texture of Materials (Ministry of Education), School of Materials Science and Engineering, Northeastern University, Shenyang 110819, China

* Correspondence: zhuq@smm.neu.edu.cn; Tel.: +86-24-8367-2700

Abstract: Traditional roadway lighting is intended to provide safe guidance for drivers and pedestrians, but the large-scale application of roadway lighting has resulted in significant energy consumption and light pollution. However, road markings prepared by luminous coating are a kind of multi-functional road marking that can meet the needs of highway lighting at night and save energy. Here, $\text{CaAl}_2\text{O}_4:\text{Eu}^{2+},\text{Nd}^{3+},\text{Gd}^{3+}$ blue long-afterglow phosphor is obtained by the high-temperature solid-state method, and the blue luminescent coating is synthesized by the blending method. The phase composition, microscopic morphology, luminescence properties and water resistance of the phosphor and luminescent coatings are characterized. The best components and processes of the luminescent coating are explored to meet the application of an expressway. Considering the afterglow's performance, the optimal calcination temperature of the phosphor is determined to be 1300 °C. The afterglow of the phosphor can be over 8 h after 2 h of daylight excitation. The addition of 1.25% SiO_2 to the luminescent coating improves the uniformity of the components, and the incorporation of 3.5% CaCO_3 improves the denseness of the coating. When the coating thickness is 0.8mm, the luminescent coating can achieve the best luminous effect. After 120 h of immersion in water, the afterglow intensity of the luminescent coating reduced to 70% of the original, which has excellent water resistance. The blue luminescent coating with the addition of appropriate amounts of CaCO_3 and SiO_2 improves the dispersion as well as the densification of the components in the coating to achieve the best luminescent effect. In the Shenyang area, different weather conditions (cloudy, sunny, rainy) have no significant effect on the afterglow performance of the luminescent coatings, all of which can achieve over 5 h of afterglow and are suitable for expressways.



Citation: Li, X.; Chen, R.; Xiao, R.; Li, W.; Si, T.; Li, P.; Zhu, Q. Natural Light Rechargeable Night Peal-like Coatings for Expressway. *Coatings* **2024**, *14*, 566. <https://doi.org/10.3390/coatings14050566>

Academic Editor: Ihor S. Virt

Received: 29 March 2024

Revised: 29 April 2024

Accepted: 30 April 2024

Published: 2 May 2024



Copyright: © 2024 by the authors. Licensee MDPI, Basel, Switzerland. This article is an open access article distributed under the terms and conditions of the Creative Commons Attribution (CC BY) license (<https://creativecommons.org/licenses/by/4.0/>).

1. Introduction

Long-afterglow materials are functional materials that emit light and store energy when excited by an external light source and release the energy in the form of ultraviolet, visible or near-infrared light after cessation of excitation [1]. Currently, a large number of phosphors with excellent afterglow properties have been reported, such as $\text{Ba}_5\text{Si}_8\text{O}_{21}:\text{Eu}^{2+},\text{Dy}^{3+}$ (blue) [2], $\text{CaAl}_2\text{O}_4:\text{Eu}^{2+},\text{Nd}^{3+}$ (blue) [3], $\text{SrAl}_2\text{O}_4:\text{Eu}^{2+},\text{Dy}^{3+}$ (green) [4], $\text{Ba}_2\text{SiO}_4:\text{Eu}^{2+},\text{Ho}^{3+}$ (green) [5], $\text{BaSiO}_3:\text{Eu}^{2+},\text{Nd}^{3+},\text{Tm}^{3+}$ (yellow) [6], $\text{SrSc}_2\text{O}_4:\text{Pr}^{3+}$ (yellow) [7], $\text{BaZnGeO}_4:\text{Bi}^{3+}$ (orange) [8], $\text{LiGaO}_2:\text{Mn}^{2+}$ (orange) [9], $\text{LiYGeO}_4:\text{Eu}^{3+}$ (red) [10] and $\text{MgGeO}_3:\text{Mn}^{2+}$ (red) [11]. The luminescent properties of these phosphors are summarized in Table S1. Due to the characteristics of a rich luminous color, long afterglow time and high stability, long-afterglow phosphors have been widely used in the fields of high-energy ray detection, information storage and lighting [12–14]. Since the 21st century, long-afterglow phosphors have received much attention for luminescent coatings. A road marking made of luminescent coating does not use any electricity, yet it can store the absorbed external light source, showing a bright light in the darkness. It can play the role of directional lighting and is a green light source material [15].

For luminous road markings, the demand for blue luminescent coatings is huge [16]. As an important component of luminescent coatings, long-afterglow phosphor determines the luminescent color, afterglow brightness and afterglow time of the coatings [17]. Nowadays, many researchers have devoted themselves to the development of blue long-afterglow phosphors, which has greatly promoted the application of luminescent coatings in road markings [18–20]. In order to achieve high-quality luminous marking, the prepared luminescent coating needs to meet the requirements to produce a long-term visible afterglow after daylight irradiation. The $\text{CaAl}_2\text{O}_4:\text{Eu}^{2+},\text{Nd}^{3+}$ long-afterglow phosphor is a kind of material that can emit blue afterglow after excitation by daylight, and the appropriate amount of Gd^{3+} will increase the trap depth and concentration in the material and improve the afterglow performance [21]. Therefore, $\text{CaAl}_2\text{O}_4:\text{Eu}^{2+},\text{Nd}^{3+},\text{Gd}^{3+}$ is used as a phosphor for the preparation of blue luminescent coatings. In this paper, a $\text{CaAl}_2\text{O}_4:\text{Eu}^{2+},\text{Nd}^{3+},\text{Gd}^{3+}$ phosphor is used for the first time to produce long-afterglow luminescent coatings for road markings, instead of proposing a new type of phosphors. However, the development of luminescent coatings for road markings is in the exploratory stage, and many issues still need to be solved. For instances, the preparation of luminous coatings by mixing phosphors into the coatings fails to reach the desirable luminescence phenomenon. Therefore, research on the composition and preparation process of luminescent coatings has become a hot topic [22]. Considering the light transmittance, an acrylic emulsion is selected as the film-forming material to prepare the luminescent coating. The homogeneity and the denseness of the luminescent coating are improved by doping with SiO_2 and CaCO_3 . The thickness of the coating is regulated to obtain a blue luminescent coating with the best afterglow performance. The research focus of the paper is about the development of a new type of blue long-afterglow luminescent coating, which will be prepared into luminescent road markings for highway applications. This kind of road marking can meet the demand of road lighting and save electricity.

In this work, we synthesized the $\text{CaAl}_2\text{O}_4:\text{Eu}^{2+},\text{Nd}^{3+},\text{Gd}^{3+}$ phosphor with good crystallization under a reducing atmosphere. The blue luminescent coatings were obtained by mixing $\text{CaAl}_2\text{O}_4:\text{Eu}^{2+},\text{Nd}^{3+},\text{Gd}^{3+}$ phosphor, acrylic emulsion, SiO_2 , CaCO_3 and additives using the blending method. The phase purity and morphology of the phosphor and coatings were characterized by X-ray diffraction (XRD) and field emission scanning electron microscopy (FE-SEM). The luminescent performance was characterized by photoluminescence excitation (PLE) spectra, photoluminescence (PL) spectra, afterglow emission spectra and afterglow decay curves. The densification of the coating was characterized by water absorption. By regulating the content of each component, blue luminescent coatings with excellent performance were successfully prepared for the expressway.

2. Experimental Section

2.1. Preparation of Phosphor

The phosphor $\text{Ca}_{1-x-y-z}\text{Al}_2\text{O}_4:x\text{Eu}^{2+},y\text{Nd}^{3+},z\text{Gd}^{3+}$ ($x = 0.012$, $y = 0.006$, $z = 0.036$) was prepared by the high-temperature solid-state method. The raw materials with a purity of 99.99% (CaCO_3 , Al_2O_3 , H_3BO_3 , Eu_2O_3 , Nd_2O_3 and Gd_2O_3) were acquired from Sinopharm. Based on stoichiometric composition, the ingredients were weighed, and then H_3BO_3 was added as the solvent. The uniformly mixed raw materials were calcined at 1300–1400 °C for 5 h in a reductive atmosphere (10% H_2 /90% N_2) to produce the phosphor.

2.2. Preparation of Luminescent Coating

The acrylic emulsion, $\text{CaAl}_2\text{O}_4:\text{Eu}^{2+},\text{Nd}^{3+},\text{Gd}^{3+}$ phosphor, filler and additives were mixed together by the blending method to obtain luminescent coatings with excellent performance. The acrylic emulsion and additives were obtained from Hebei Taiji Chemical Industry and Jitian Chemical Industry (Shijiazhuang, China), respectively. The fillers were SiO_2 (A.R.) and CaCO_3 (A.R.) purchased from Sinopharm. According to the mass ratio of materials, the reagents were weighed. First, water, thickening agent, SiO_2 and CaCO_3 were put into the beaker and stirred, and then the film-forming agent and acrylic emulsion were

added. After mixing for 15 min, the anti-sedimentation agent, $\text{CaAl}_2\text{O}_4:\text{Eu}^{2+},\text{Nd}^{3+},\text{Gd}^{3+}$ phosphor and silane coupling agent were combined and stirred for 10 min to obtain the blue luminescent coating.

2.3. Characterization Techniques

The phase of the samples was verified by X-ray diffraction (XRD, Model SmartLab, Rigaku, Tokyo, Japan), and the diffraction data were measured with nickel-filtered $\text{Cu K}\alpha$ radiation. The scanning range of samples performed at a scanning speed of $8.0^\circ 2\theta/\text{min}$ was 10° to 60° . The morphology at an accelerating voltage of 15 kV was observed with a field emission scanning electron microscope (FE-SEM, Model S-4800, Hitachi, Tokyo, Japan). The PLE spectra, PL spectra, afterglow emission spectra and afterglow decay curves were measured by spectrophotometer (Model JY FL3-21, Horiba, Kyoto City, Japan). The thermoluminescence (TL) glow curve was obtained on a spectrometer (Model FJ-427A TL, Beijing Nuclear Instrument Factory, Beijing, China) with a heating rate of $1 \text{ K}\cdot\text{s}^{-1}$. Before the TL measurements, the phosphor was placed under 365 nm UV and irradiated for 5 min.

3. Results and Discussion

Figure 1a is the XRD patterns of blue $\text{CaAl}_2\text{O}_4:\text{Eu}^{2+},\text{Nd}^{3+},\text{Gd}^{3+}$ long-afterglow phosphors calcined at different temperatures. It can be observed that the diffraction peaks of each phosphor are completely consistent with the standard CaAl_2O_4 card (JCPDS No. 70-0134), indicating that pure-phase samples calcined at 1300°C , 1350°C and 1400°C have been obtained. In Figure 1b, elemental mapping images confirm that the particle size of the sample calcined at 1300°C is about $10 \mu\text{m}$, and the elements (Ca, Al, Eu, Nd and Gd) are uniformly distributed in the particle.

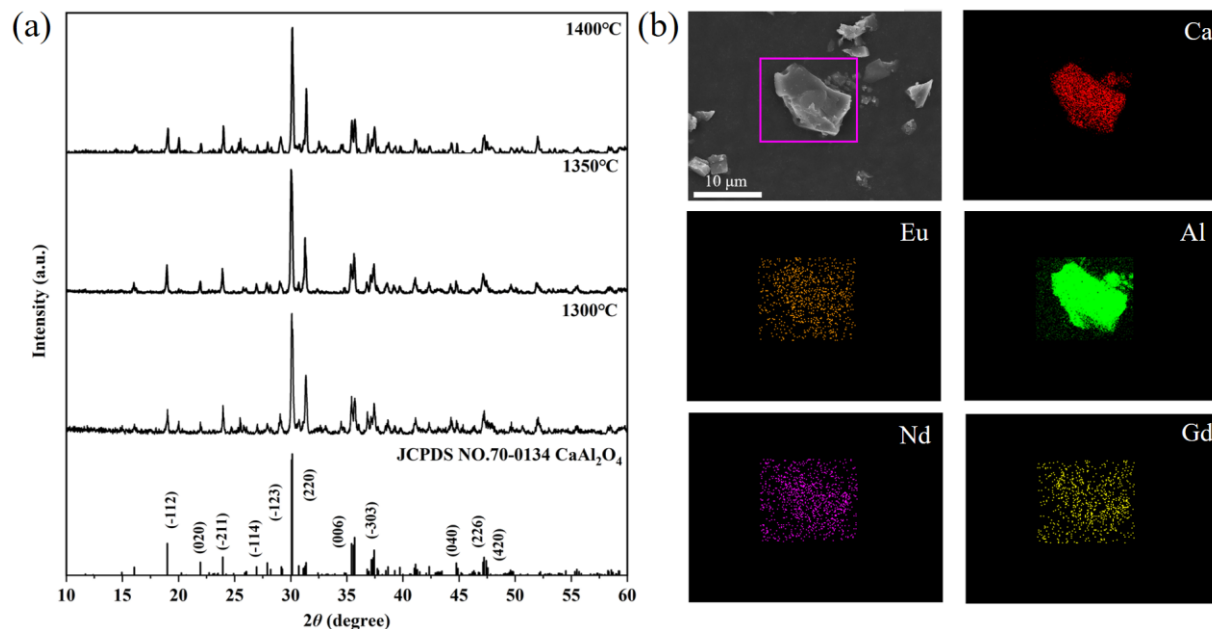


Figure 1. (a) XRD patterns of $\text{CaAl}_2\text{O}_4:\text{Eu}^{2+},\text{Nd}^{3+},\text{Gd}^{3+}$ calcined at different temperatures. (b) Elemental mapping images of Ca, Al, Eu, Nd and Gd for the selected particle calcined at 1300°C .

Figure 2a presents the PLE spectra of $\text{CaAl}_2\text{O}_4:\text{Eu}^{2+},\text{Nd}^{3+},\text{Gd}^{3+}$ phosphor calcined at $1300\text{--}1400^\circ\text{C}$. The PLE spectra of all samples monitored at 442 nm contain a broad band of $250\text{--}400$ nm with a maximum around 355 nm. Therefore, sunlight can effectively excite the phosphor. As can be seen from the photoluminescence (PL) spectra in Figure 2b, all samples exhibit a blue emission at 442 nm excited by UV light at 355 nm, attributed to the $5\text{d}^1\text{-}4\text{f}^7$ transition of Eu^{2+} [21]. Furthermore, the intensity of the phosphors decreases gradually with the increase in calcination temperature, and the sample calcined at 1300°C has the

highest phosphorescent intensity. Figure 2c displays the afterglow spectra of phosphors excited by 365 nm UV lamp. The emission wavelength of the afterglow is 442 nm, similar to the PL spectra. Figure 2d shows the afterglow decay curves of the $\text{CaAl}_2\text{O}_4:\text{Eu}^{2+},\text{Nd}^{3+},\text{Gd}^{3+}$ phosphor calcined at 1300–1400 °C. The afterglow duration becomes shorter and the intensity of the afterglow becomes weaker as the calcination temperature increases, and the sample calcined at 1300 °C has the optimal afterglow performance. In the long-afterglow materials, the trap plays an essential role in the generation of afterglow [23,24]. In order to investigate the depth and concentration of traps, the thermoluminescence (TL) curves of phosphors calcined at different temperatures are tested after irradiation with a 365 nm UV lamp for 5 min (Figure 2e). The TL curves of phosphors cover a wide range of 310–380 K, including two peaks. The trap depth (E) of the phosphor can be calculated according to Formula (1) [25].

$$E = \frac{T_m}{500} \quad (1)$$

where T_m is the temperature of the peak maximum in TL curves (kelvin temperature). The depth of the trap determines the afterglow property. At room temperature, the carriers in the shallow trap are more easily released, resulting in higher initial afterglow intensity, while deep traps cause a long-lasting afterglow [26,27]. Compared with the sample obtained at 1350 °C and 1400 °C, the phosphor obtained at 1300 °C has two traps at 0.66 eV and 0.74 eV, and appropriate trap depth makes it have the best afterglow initial intensity and afterglow duration. Therefore, the optimum calcination temperature of $\text{CaAl}_2\text{O}_4:\text{Eu}^{2+},\text{Nd}^{3+},\text{Gd}^{3+}$ blue phosphor is determined to be 1300 °C. The afterglow emission color is analyzed by using CIE chromaticity diagram, indicating that the color is positioned in the blue area with coordinates of (0.147, 0.058) in Figure 2f. In the dark, the naked eye can see a blue afterglow that lasts for more than 8 h (Figure 2g).

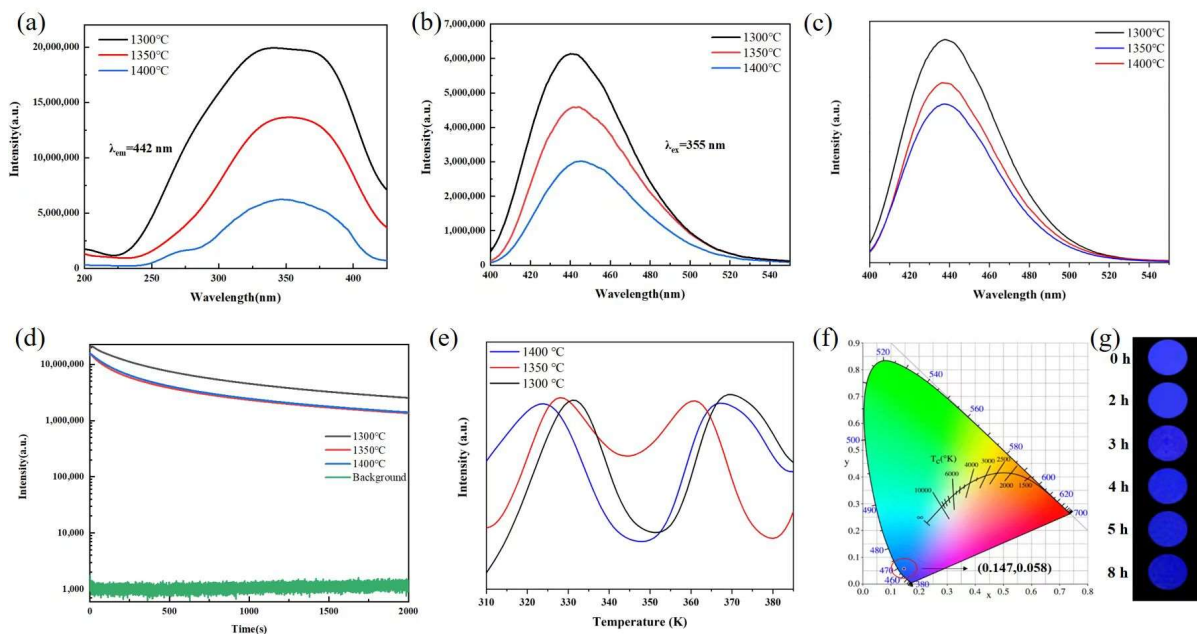


Figure 2. (a) PLE spectra and (b) PL spectra of $\text{CaAl}_2\text{O}_4:\text{Eu}^{2+},\text{Nd}^{3+},\text{Gd}^{3+}$ phosphor calcined at different temperatures. (c) Afterglow spectra, (d) afterglow decay curve and (e) TL glow curve of $\text{CaAl}_2\text{O}_4:\text{Eu}^{2+},\text{Nd}^{3+},\text{Gd}^{3+}$ phosphor calcined at different temperatures. (f) CIE chromaticity coordinates and (g) afterglow images of $\text{CaAl}_2\text{O}_4:\text{Eu}^{2+},\text{Nd}^{3+},\text{Gd}^{3+}$ phosphor calcined at 1300 °C after sunlight excitation for 2 h.

The blue luminous coating obtained using the blending method is coated on the substrate. After drying at room temperature, the blue luminous coating is obtained (Figure 3). Then, the luminescence performance, uniformity and water resistance of the coating can be discussed in detail.

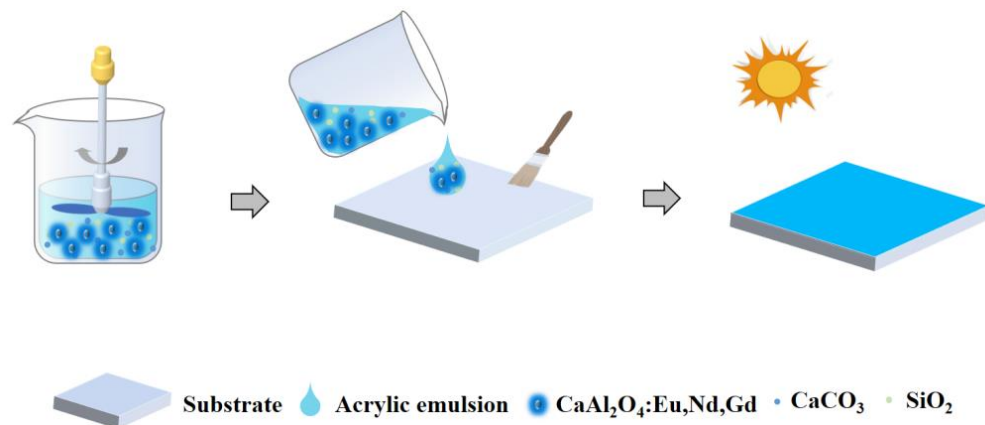


Figure 3. Schematic illustration of the preparation process of luminescent coating.

As shown in Figure 4a, the diffraction peaks of the blue coating perfectly correspond to the diffraction peaks of the CaAl₂O₄:Eu²⁺,Nd³⁺,Gd³⁺ phosphor in XRD patterns. This indicates that the crystal structure of the CaAl₂O₄:Eu²⁺,Nd³⁺,Gd³⁺ phosphor does not change after the preparation of luminescent coatings [28]. Figure 4b shows the element mapping analysis of the blue coating cross-section, indicating that Ca, Al, C, O and Si elements are detected, which further indicates that CaAl₂O₄:Eu²⁺,Nd³⁺,Gd³⁺, SiO₂ and CaCO₃ are distributed in the film-forming material, and the blue coating with uniformly dispersed components is obtained.

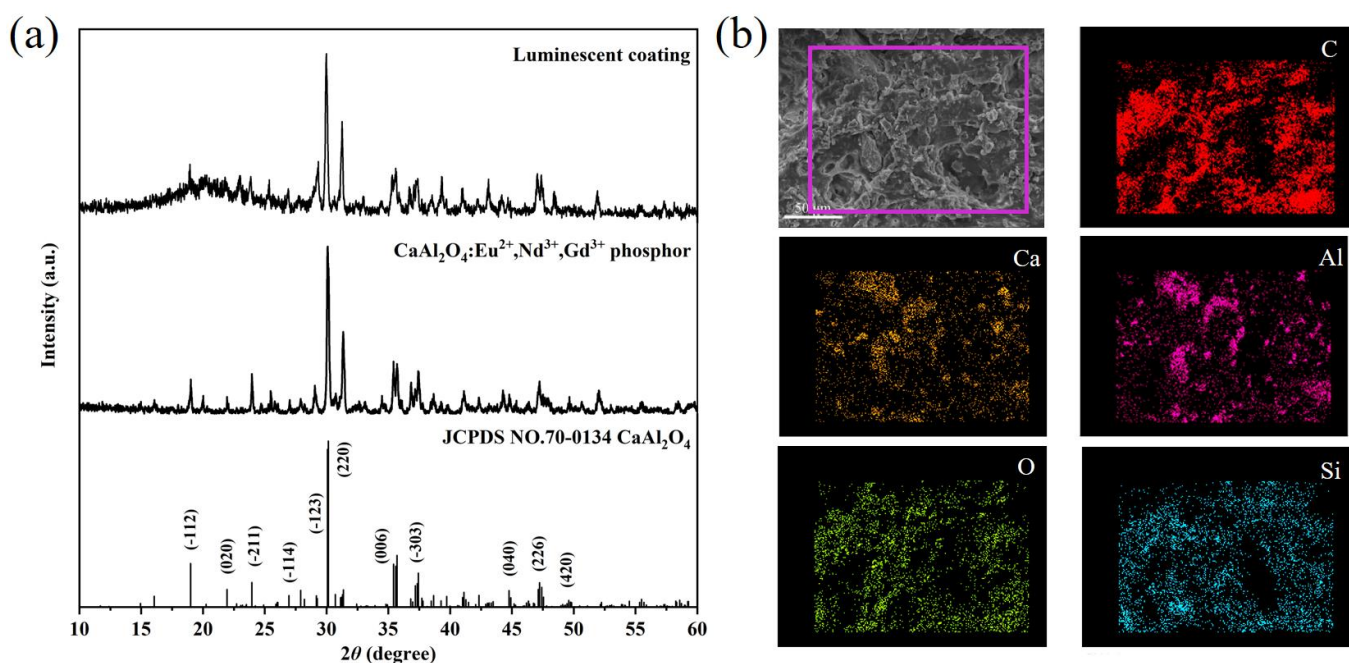


Figure 4. (a) XRD patterns of CaAl₂O₄:Eu²⁺,Nd³⁺,Gd³⁺ phosphor and luminescent coating. (b) FE-SEM image and elemental mapping images of C, Ca, Al, Si and O for cross section of luminescent coating.

Figure 5 shows FE-SEM images of blue coating sections with different SiO_2 contents. It can be concluded that proper SiO_2 addition leads to the dispersion of the components in the luminescent coating [29,30]. The pores in the luminescent coating cross sections look similar after doping with 0.75%–1.25% SiO_2 . And it can be clearly seen that pores appear in the layers at 0.5% and 1.5% SiO_2 doping. The optimum SiO_2 content of 1.25% is determined from the emission intensity in the PL spectra in Figure S1.

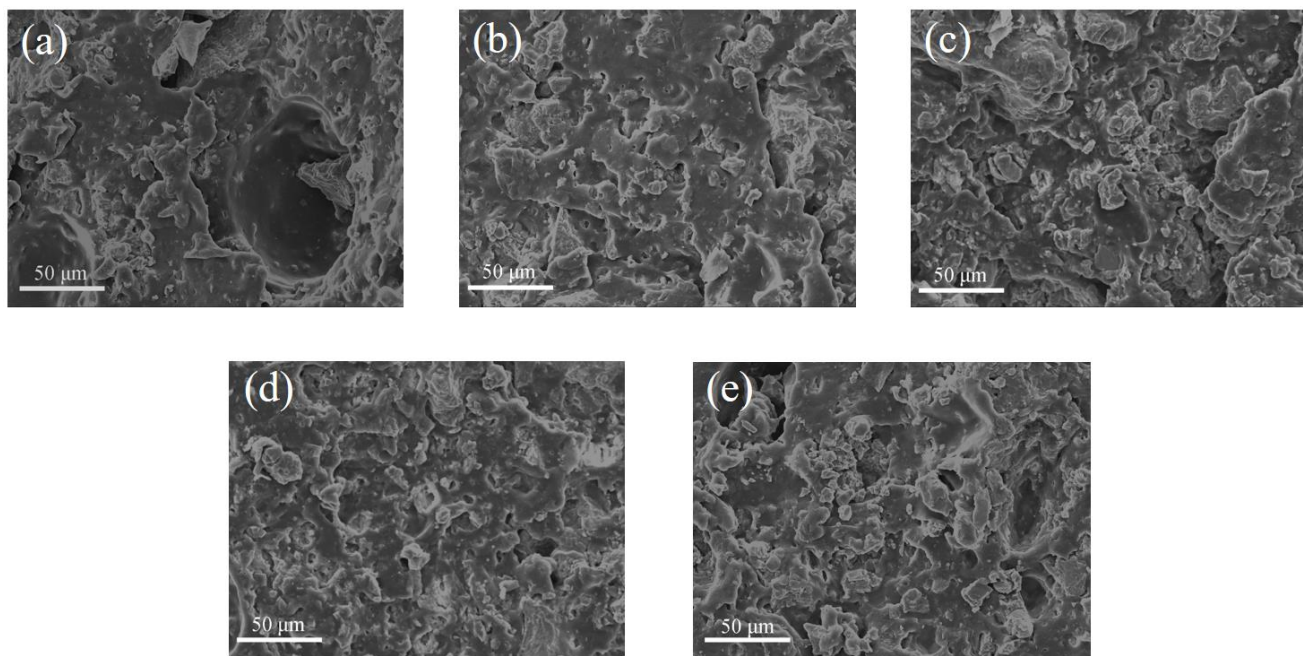


Figure 5. FE-SEM images of luminescent coating cross sections with different SiO_2 contents: (a) 0.5%, (b) 0.75%, (c) 1%, (d) 1.25% and (e) 1.5%.

The water absorption of blue coatings after the addition of CaCO_3 is measured systematically. The dry luminescent coatings are weighed and then soaked in deionized water for varying durations. After taking them out, the surface water of the coatings is drained by filter paper and weighed, and then the water absorption is calculated by Equation (2) [31,32].

$$m_t = \frac{(m_2 - m_1)}{m_1} 100\% \quad (2)$$

where m_t is the water absorption of the coating, m_1 is the mass of the coating before immersion and m_2 is the mass of the coating after immersion. As illustrated in Figure 6a, the water absorption curve trend of the blue coatings can be classified into two stages. In the first stage, the water absorption of the coating increases with the duration of immersion, and about 5 days later, it remains stable and reaches saturation. The coating containing 3.5% CaCO_3 has the lowest water absorption, close to 28%. Figure 6b is the diagram obtained by nonlinear fitting of the initial water absorption, and it is calculated that the n value of luminescent coatings with different CaCO_3 contents is close to 0.5, and the fitting data are seen in Table S2. It can be concluded that at the start of immersion, the diffusion behavior of water in the luminescent coating is consistent with the ideal Fick diffusion. Therefore, the diffusion coefficient D can be obtained from the following Formula (3) [33,34].

$$\frac{m_t}{m_s} = \frac{4\sqrt{D}}{L\sqrt{\pi}} \sqrt{t} \quad (3)$$

where m_t is the water absorption of the coating at time t , m_s is the water absorption when the coating is saturated, D is the diffusion coefficient ($\text{cm}^2 \cdot \text{s}^{-1}$) and L is the coating thickness

(cm). Figure 7 indicates that the diffusion coefficient of water in the coating increases and then decreases as the filler content increases and the addition of 3.5% CaCO_3 is the lowest. Further, the density of the blue coating can be enhanced by adding the appropriate filler CaCO_3 .

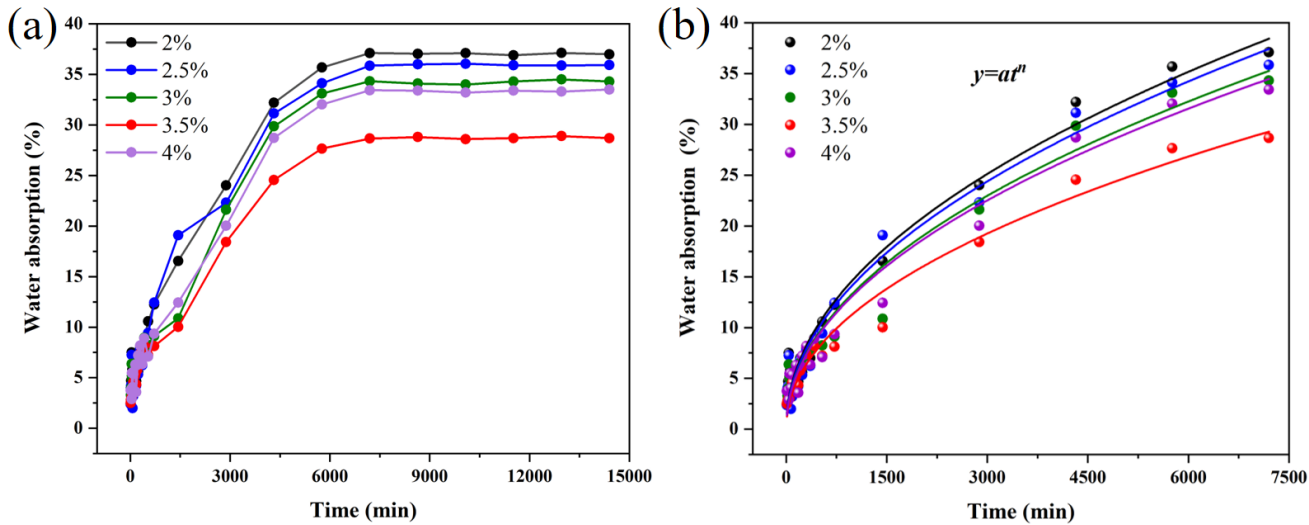


Figure 6. (a) Water absorption and (b) the fitting diagram of the water absorption of luminescent coatings with different CaCO_3 contents.

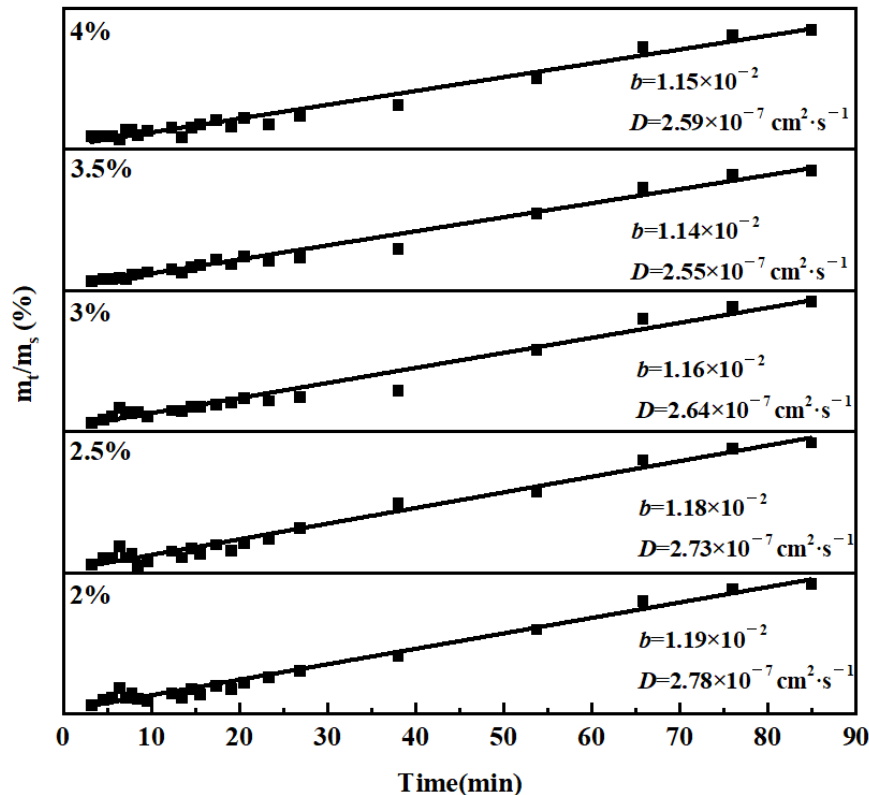


Figure 7. The relationship between water absorption and immersion time of luminescent coatings with different CaCO_3 contents.

Figure 8 shows the FE-SEM images of the coating surfaces' different contents of phosphors, and it can be seen that all surfaces of the luminescent coatings are flat and compact with no pores. Therefore, blue luminescent coatings will not cause light scattering and low light absorption due to surface defects, which is conducive to light storage of luminous coatings. Normally, the flatness of the coating is affected by mixing different phosphor contents. However, in our experiments, the phosphors were embedded in the film-forming substance acrylic emulsion, so that the morphology observed through the FE-SEM images of the coating surface was basically the same.

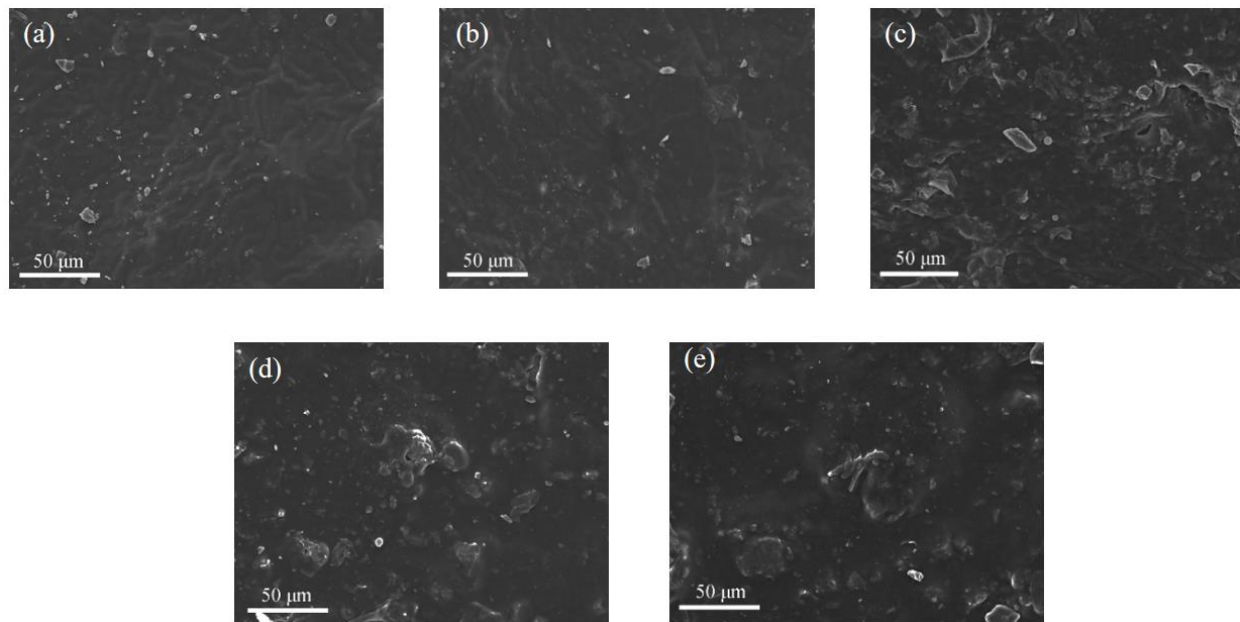


Figure 8. FE-SEM images of luminescent coating surfaces with different ratios of phosphor to emulsion: (a) 1:1, (b) 1:1.5, (c) 1:2, (d) 1:2.5, (e) 1:3.

Figure 9a exhibits the PLE spectra of blue coatings prepared by different ratios of phosphor to emulsion, from which it can be seen that the spectra cover from 300 nm to 400 nm, peaking at about 355 nm. Thus, sunlight can effectively excite the coating. Under 355 nm excitation, all the coatings show characteristic emissions of Eu^{2+} with a maximum emission peak of about 442 nm (Figure 9b), which belongs to the $5\text{d}^1-4\text{f}^7$ transition of Eu^{2+} . This indicates that the basic luminescent properties of the $\text{CaAl}_2\text{O}_4:\text{Eu}^{2+}, \text{Nd}^{3+}, \text{Gd}^{3+}$ do not change after added phosphor to the coating. With the increase in phosphor content, the intensity of emission peaks of the luminescent coatings first increased and then decreased. In theory, with the increase in the amount of phosphor, the luminous brightness of the coating will increase. This difference is caused by the fact that when there is too much phosphor in the coating, the phosphor will accumulate and lead to uneven dispersion, which makes it difficult to achieve a rational luminous effect. Therefore, we need to add the appropriate content of phosphor, which can both make it evenly dispersed in the luminescent coating and meet the luminous requirements. Figure 9c shows the afterglow spectra of the coatings, and the afterglow of all coatings emits blue light at 442 nm. It is observed from the afterglow decay curves of the luminescent coatings in Figure 9d that the intensity of the coating is the highest when the ratio of phosphor to emulsion is 1:1.5. Therefore, the best ratio of phosphor to emulsion in this experiment is 1:1.5.

The PLE spectra in Figure S1a monitored the emissions at 442 nm, covering a wide band centered around 355 nm. Figure S1b displays the PL spectra measured at 355 nm excitation; the spectra include a broad band of 400–500 nm with a maximum of 442 nm. The addition of SiO_2 will not affect the basic characteristics of the luminescence of the coating, and the reduction in emission intensity occurs when the content of SiO_2 exceeds

1.25% in the luminescent coatings. The afterglow spectra and afterglow decay curves are shown in Figure S1c,d, which are detected after removing the 365 nm excitation resource. It can be seen that the afterglow intensity is highest with the addition of 1.25% SiO₂. This is because appropriate addition of SiO₂ can make the components in the luminescent coating dispersion more uniform, thus obtaining a coating with optimum luminescent properties.

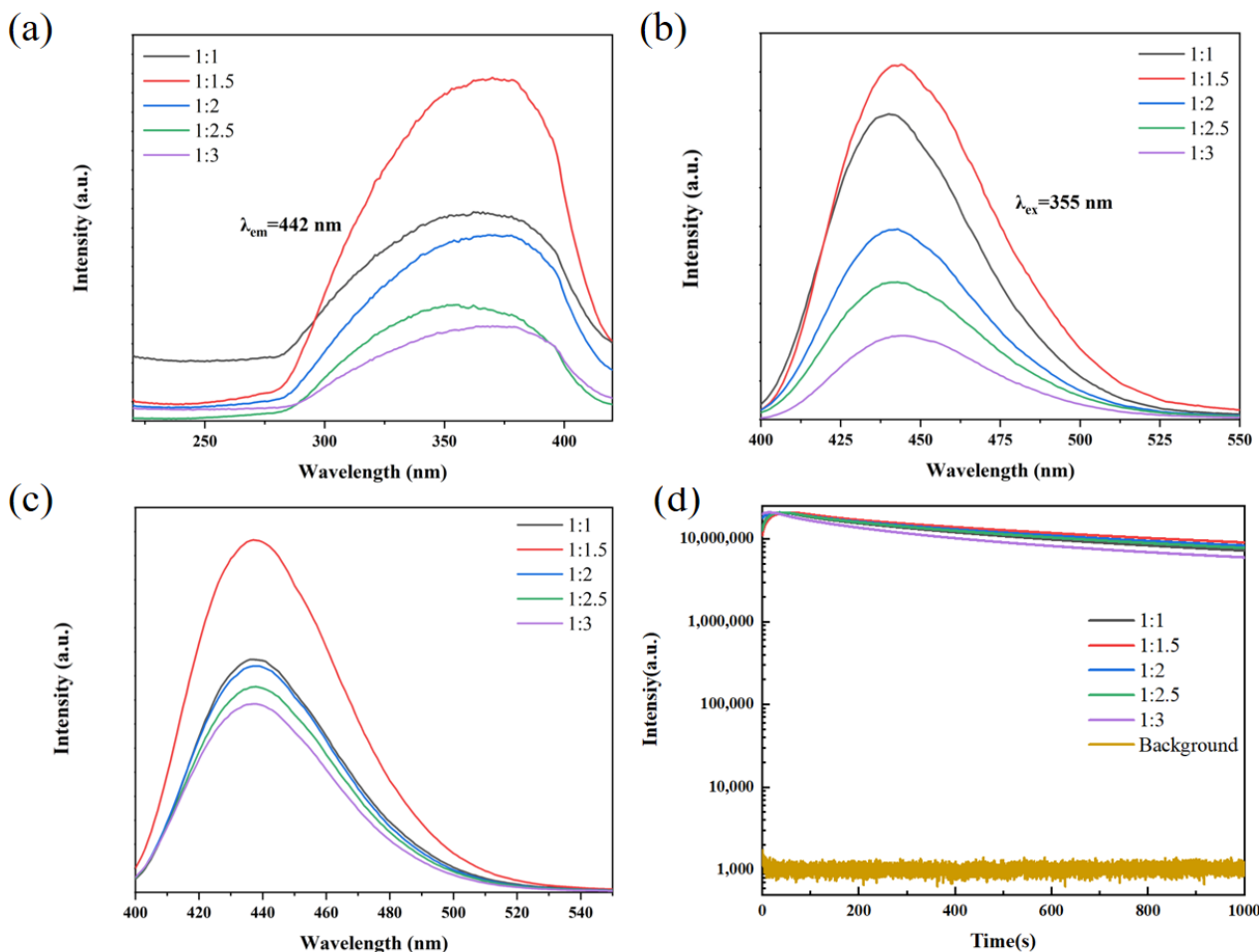


Figure 9. (a) PLE spectra and (b) PL spectra of luminescent coatings with different ratios of phosphor to emulsion. (c) Afterglow spectra and (d) afterglow decay curves of luminescent coatings with different ratios of phosphor to emulsion obtained after 5 min illumination with 365 nm UV light.

It can be seen that the profiles of PLE and PL spectra of the luminescent coatings (Figure S2a,b) do not show changes after the addition of filler CaCO₃, and the afterglow spectra in Figure S2c include a broad band located with emissions at 442 nm. The intensity of the coatings decreases quickly within the first 15 min and then declines slowly (Figure S2d). It can be observed that the afterglow intensity is highest when the CaCO₃ addition is 3.5%. This is because after adding the appropriate content of CaCO₃, the coating has the best density, which is conducive to the phosphor to achieve the best luminescence. Therefore, the optimal incorporation content of the CaCO₃ in the blue luminescent coating is determined to be 3.5%.

Figure 10 exhibits photographs of the afterglow of blue coatings with different compositions; it is observed that after 2 h of excitation by daylight, the coating will produce a blue afterglow for more than 5 h. By adjusting the content of phosphor, SiO₂ and CaCO₃ in the luminescent coating, the dispersion and density of the coating are improved, and finally the coating with the best luminescent performance is obtained. The blue channel values for these photos are shown in Tables S3–S5. After determining the best content of each component, the influence of the thickness of the blue luminescent coating on the

luminous property is investigated. Figure S3a,b are the PLE and PL spectra of the coatings with different thicknesses, respectively; the excitation and emission intensity are highest at a thickness of 0.8 mm. Figure S3c,d show that as the thickness increases, the afterglow intensity of the blue coating first increases and then decreases. This indicates that when the thickness of the luminescent coating is too thick, the $\text{CaAl}_2\text{O}_4:\text{Eu}^{2+},\text{Nd}^{3+},\text{Gd}^{3+}$ in the lower layer of the coating is blocked when receiving irradiation from external light sources, which leads to the afterglow brightness of the coating being reduced. Figure S3e is the afterglow photos of different thicknesses of coatings after excitation by daylight, and the highest brightness in the thickness of 0.8 mm. Therefore, the optimal thickness of the luminescent coating is 0.8 mm.

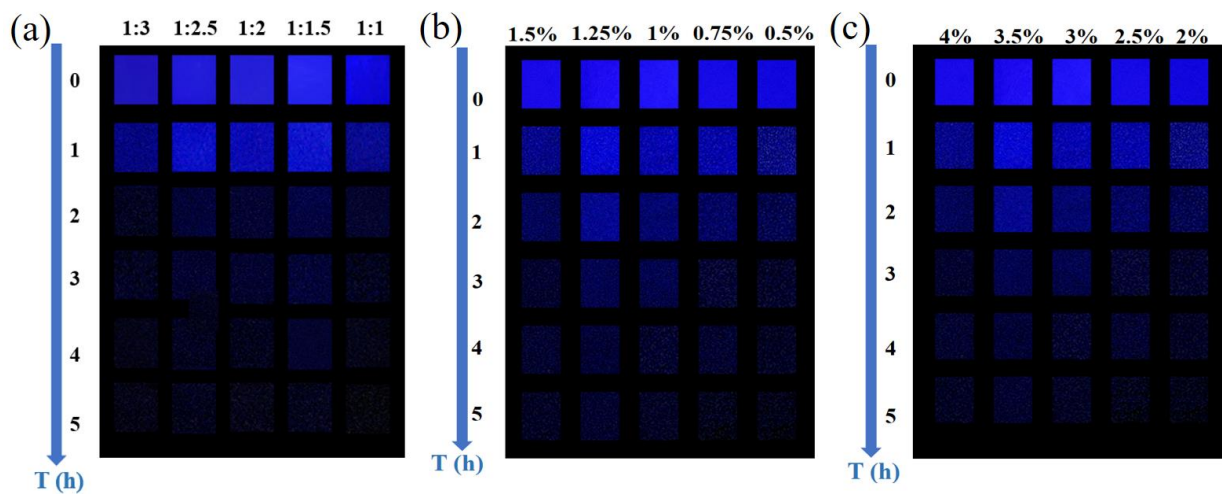


Figure 10. Afterglow decay images of luminescent coatings taken after sunlight excitation for 2 h (a) with different ratios of phosphor to emulsion, (b) with different SiO_2 contents and (c) with different CaCO_3 contents.

In order to meet the actual application, the blue coatings should have good water resistance. After 120 h of immersion in water, the surfaces of the coatings are flat and smooth without blistering. (Figure 11a). According to the afterglow spectra in Figure 11b, the basic luminescence characteristics of the luminescent coating are unchanged after the coating is soaked in water. Figure 11c indicates that the afterglow intensity of the coating slowly reduces with increasing immersion time. After 120 h of immersion, the coating still produces a bright blue afterglow after 10 s of UV excitation at 365 nm. Figure 11d depicts the change in afterglow intensity at different time lengths after immersion. The intensity decreases faster at the beginning of immersion and decreases more slowly after 96 h of immersion in water. After 120 h of immersion in water, the afterglow intensity at 1000 s still reaches 70% of that of the unsoaked coating. It shows that the coating has good waterproof performance.

Figure 12 is the photographs of the afterglow of the coatings after 2 h of daylight excitation at 10 a.m. in Shenyang ($123^{\circ}23' \text{ E}$, $41^{\circ}48' \text{ N}$) with cloudy, sunny and rainy conditions. The blue channel values for these photos are shown in Table S6. The afterglow intensity of the luminescent coating achieved under different weather conditions does not differ much, and the duration of the blue afterglow can last over 5 h. This means that weather conditions have no effect on it, so the blue luminous coating is suitable for expressways.

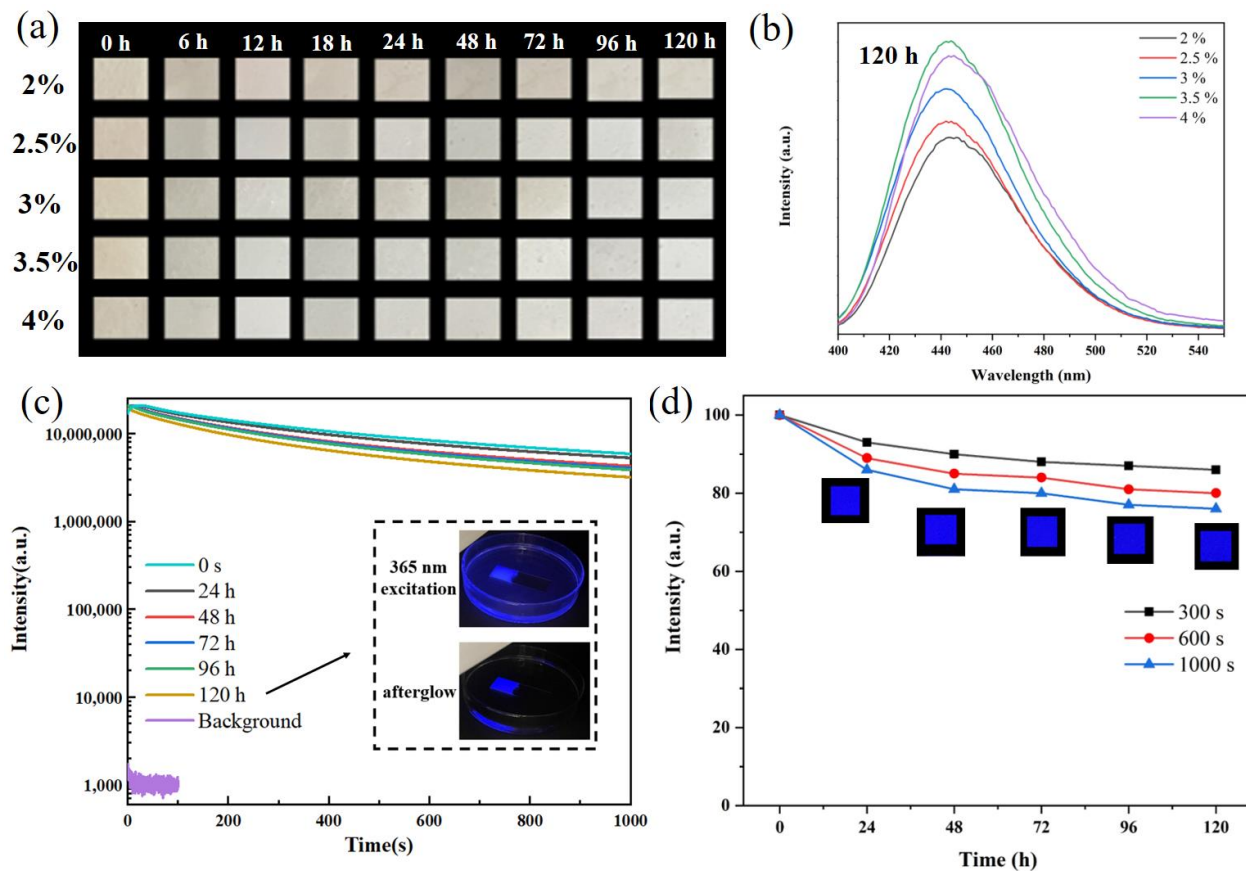


Figure 11. (a) Photographs of luminescent coatings with different CaCO_3 contents after immersion in water. (b) Afterglow spectra of luminescent coatings with different CaCO_3 contents after immersion in water for 120 h obtained with 5 min illumination of 365 nm UV light. (c) Afterglow decay curves of 3.5% CaCO_3 -doped luminescent coating after immersion in water for different times obtained after 5 min illumination with 365 nm UV light. The inset is the afterglow image of 3.5% CaCO_3 -doped luminescent coating after immersion in water for 120 h taken after 10 s illumination with 365 nm UV light. (d) The change rate of afterglow intensity of 3.5% CaCO_3 -doped luminescent coating after immersion in water for different times. The inset is the afterglow images at 1000 s after excitation.

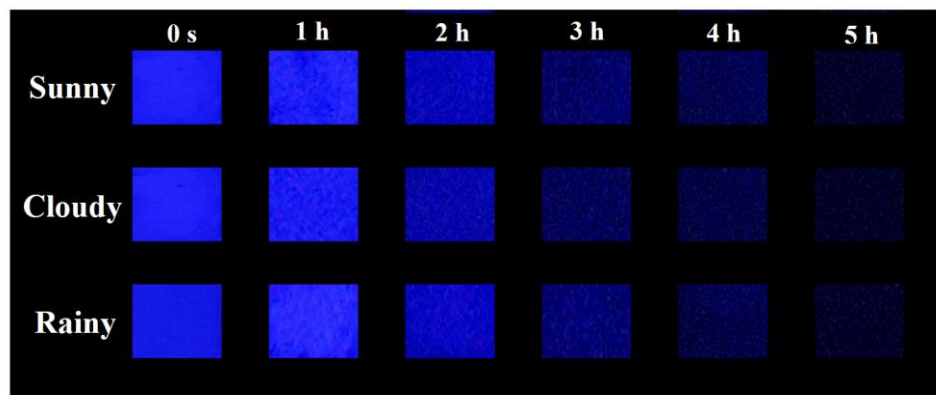


Figure 12. Afterglow images of luminescent coatings taken after sunlight excitation for 2 h in different weather conditions.

4. Conclusions

In this work, blue $\text{CaAl}_2\text{O}_4:\text{Eu}^{2+},\text{Nd}^{3+},\text{Gd}^{3+}$ phosphor is prepared in a reducing atmosphere by the high-temperature solid-state method, and then blue luminescent coatings are synthesized by the blending method. The phase composition, microstructure, luminescence properties and water resistance are characterized to explore the optimal composition and process of luminescent coatings for highway applications. The optimal calcination temperature of the $\text{CaAl}_2\text{O}_4:\text{Eu}^{2+},\text{Nd}^{3+},\text{Gd}^{3+}$ phosphor is determined to be 1300 °C considering the afterglow performance, which is due to the fact that the phosphor prepared at this temperature has two traps at 0.66 eV and 0.74 eV. The afterglow of phosphor can be over 8 h after 2 h of daylight excitation. The optimal ratio of each component in the blue coating is obtained: the ratio of phosphor to emulsion is 1:1.5, the CaCO_3 incorporation is 3.5 wt% and the SiO_2 addition is 1.25 wt%. The appropriate addition of CaCO_3 and SiO_2 to the coating can increase the density and make the components more uniform, respectively. The optimum luminous effect is achieved when the thickness of the coating is 0.8 mm. After 120 h of immersion in water, the afterglow intensity of luminescent coating is reduced to 70% of that of the unsoaked coating, demonstrating excellent water resistance. In the Shenyang area, different weather conditions (cloudy, sunny, rainy) have no significant effect on the afterglow performance of the luminescent coatings, all of which can last over 5 h and are suitable for expressways.

Supplementary Materials: The following supporting information can be downloaded at: <https://www.mdpi.com/article/10.3390/coatings14050566/s1>, Table S1: A comparison of the luminescent properties of these phosphors; Table S2: The results of fitting data of water absorption of blue luminescent coatings with different filler CaCO_3 content; Table S3: The blue channel values of afterglow decay images of luminescent coatings with different ratios of phosphor to emulsion (in RGB format); Table S4: The blue channel values of afterglow decay images of luminescent coatings with different SiO_2 content (in RGB format); Table S5: The blue channel values of afterglow decay images of luminescent coatings with different CaCO_3 contents (in RGB format); Table S6: The blue channel values of afterglow decay images of luminescent coatings (in RGB format); Figure S1: (a) PLE spectra, and (b) PL spectra of luminescent coatings with different SiO_2 contents. (c) Afterglow spectra, and (d) Afterglow decay curves of luminescent coatings with different SiO_2 contents obtained after 5 min illumination with 365 nm UV light; Figure S2: (a) PLE spectra, and (b) PL spectra of luminescent coatings with different CaCO_3 contents. (c) Afterglow spectra, and (d) Afterglow decay curves of luminescent coatings with different CaCO_3 contents obtained after 5 min illumination with 365 nm UV light; Figure S3: (a) PLE spectra, and (b) PL spectra of luminescent coatings with different thickness. (c) Afterglow spectra, and (d) Afterglow decay curves of luminescent coatings with different thickness obtained after 5 min illumination with 365 nm UV light. (e) Afterglow images of luminescent coatings taken after sunlight excitation for 2 h, with different thickness.

Author Contributions: X.L.: data curation, formal analysis. R.C.: data curation, formal analysis. R.X.: data curation, formal analysis. W.L.: data curation, formal analysis. T.S.: data curation. P.L.: data curation, formal analysis, writing—original draft. Q.Z.: resources, supervision, conceptualization, writing—review and editing, conceptualization. All authors have read and agreed to the published version of the manuscript.

Funding: Natural Science Foundation of Liaoning Province (Grant No. 2020-MS-081).

Institutional Review Board Statement: Not applicable.

Informed Consent Statement: Not applicable.

Data Availability Statement: The raw data supporting the conclusions of this article will be made available by the authors on request.

Conflicts of Interest: Author Xin Li, Rong Chen, Rui Xiao, Wenjie Li, Te Si were employed by the company Sichuan Transportation Construction Group Co., Ltd.. The remaining authors declare that the research was conducted in the absence of any commercial or financial relationships that could be construed as a potential conflict of interest.

References

- Xu, J.; Tanabe, S. Persistent luminescence instead of phosphorescence: History, mechanism, and perspective. *J. Lumines.* **2019**, *205*, 581–620. [[CrossRef](#)]
- Wang, P.; Xu, X.; Zhou, D.; Yu, X.; Qiu, J. Sunlight activated long-lasting luminescence from Ba₅Si₈O₂₁:Eu²⁺,Dy³⁺ phosphor. *Inorg. Chem.* **2015**, *54*, 1690–1697. [[CrossRef](#)]
- Qu, B.; Zhang, B.; Wang, L.; Zhou, R.; Zeng, X. Mechanistic study of the persistent luminescence of CaAl₂O₄:Eu,Nd. *Chem. Mat.* **2015**, *27*, 2195–2202. [[CrossRef](#)]
- Matsuzawa, T.; Aoki, Y.; Takeuchi, N.; Murayama, Y. A new long phosphorescent phosphor with high brightness, SrAl₂O₄:Eu²⁺,Dy³⁺. *J. Electrochem. Soc.* **1996**, *143*, 2670. [[CrossRef](#)]
- Wang, C.; Jin, Y.; Lv, Y.; Ju, G.; Liu, D.; Chen, L.; Li, Z.; Hu, Y. Trap distribution tailoring guided design of super-long-persistent phosphor Ba₂SiO₄:Eu²⁺,Ho³⁺ and photostimulable luminescence for optical information storage. *J. Mater. Chem. C* **2018**, *6*, 6058–6067. [[CrossRef](#)]
- Jia, Y.; Sun, W.; Pang, R.; Ma, T.; Li, D.; Li, H.; Zhang, S.; Fu, J.; Jiang, L.; Li, C. Sunlight activated new long persistent luminescence phosphor BaSiO₃:Eu²⁺,Nd³⁺,Tm³⁺: Optical properties and mechanism. *Mater. Des.* **2016**, *90*, 218–224. [[CrossRef](#)]
- Fu, X.; Zheng, S.; Meng, Y.; Sun, W.; Zhang, H. Long afterglow yellow luminescence from Pr³⁺ doped SrSc₂O₄. *J. Rare Earths* **2022**, *40*, 567–571. [[CrossRef](#)]
- Sun, W.; Jiao, M.; Fan, L.; Zhang, R.; Zhang, X.; Zhang, H. Design of a defect-induced orange persistent luminescence phosphor BaZnGeO₄:Bi³⁺. *J. Am. Ceram. Soc.* **2022**, *105*, 2128–2139. [[CrossRef](#)]
- Yang, H.; Zhao, W.; Song, E.; Hu, K.; Zhang, H.; Yun, R.; Huang, H.; Zhong, J.; Li, Y.; Li, X. Efficient visible light charging for rare earth-free persistent phosphor. *Adv. Opt. Mater.* **2022**, *10*, 2102496. [[CrossRef](#)]
- Dai, T.; Ju, G.; Lv, Y.; Jin, Y.; Wu, H.; Hu, Y. Luminescence properties of novel dual-emission (UV/red) long afterglow phosphor LiYGeO₄:Eu³⁺. *J. Lumines.* **2021**, *237*, 118193. [[CrossRef](#)]
- Doke, G.; Antuzevics, A.; Krieke, G.; Kalnina, A.; Springis, M.; Sarakovskis, A. UV and X-ray excited red persistent luminescence in Mn²⁺ doped MgGeO₃ material synthesized in air and reducing atmosphere. *J. Lumines.* **2021**, *234*, 117995. [[CrossRef](#)]
- Long, J.; Yuan, X.; Ma, C.; Du, M.; Ma, X.; Wen, Z.; Ma, R.; Wang, Y.; Cao, Y. Strongly enhanced luminescence of Sr₄Al₁₄O₂₅:Mn⁴⁺ phosphor by co-doping B³⁺ and Na⁺ ions with red emission for plant growth LEDs. *RSC Adv.* **2018**, *8*, 1469–1476. [[CrossRef](#)]
- Zhuang, Y.; Chen, D.; Chen, W.; Zhang, W.; Su, X.; Deng, R.; An, Z.; Chen, H.; Xie, R. X-ray-charged bright persistent luminescence in NaYF₄:Ln³⁺@NaYF₄ nanoparticles for multidimensional optical information storage. *Light Sci. Appl.* **2021**, *10*, 132. [[CrossRef](#)]
- Zhuang, Y.; Wang, L.; Lv, Y.; Zhou, T.; Xie, R. Optical data storage and multicolor emission readout on flexible films using deep-trap persistent luminescence materials. *Adv. Funct. Mater.* **2018**, *28*, 1705769. [[CrossRef](#)]
- Tian, S.; Wen, J.; Fan, H.; Chen, Y.; Yan, J. A thermochromic luminous polyurethane based on long persistent luminescent phosphors and thermochromic pigment. *New J. Chem.* **2018**, *42*, 5066–5070. [[CrossRef](#)]
- Rojas-Hernandez, R.; Rubio-Marcos, F.; Rodriguez, M.; Fernandez, J. Long lasting phosphors: SrAl₂O₄:Eu,Dy as the most studied material. *Renew. Sust. Energ. Rev.* **2018**, *81*, 2759–2770. [[CrossRef](#)]
- Kalyani, N.T.; Jain, A.; Dhoble, S. Persistent phosphors for luminous paints: A review. *Luminescence* **2022**, *37*, 524–542. [[CrossRef](#)]
- Finley, E.; Cobb, A.; Duke, A.; Paterson, A.; Brigoch, J. Optimizing blue persistent luminescence in (Sr_{1-δ}Ba_δ)₂MgSi₂O₇:Eu²⁺,Dy³⁺ via solid solution for use in point-of-care diagnostics. *ACS Appl. Mater. Interfaces* **2016**, *8*, 26956–26963. [[CrossRef](#)]
- Xiao, L.; Zhou, J.; Liu, G.; Wang, L. Luminescent properties of R⁺ doped Sr₂MgSi₂O₇:Eu²⁺,Dy³⁺ (R⁺ = Li⁺, Ag⁺) phosphors. *J. Alloy. Compd.* **2017**, *712*, 24–29. [[CrossRef](#)]
- Guo, H.; Wang, Y.; Li, G.; Feng, P.; Liu, D.; Ye, Q. Activating persistent luminescence and thermal stability of K₂Ba₇Si₁₆O₄₀:Eu²⁺ via traps modulation. *J. Alloy. Compd.* **2019**, *801*, 295–301. [[CrossRef](#)]
- Zhang, M.; Li, F.; Lin, Y.; Li, Y.; Shen, Y. Enhanced afterglow performance of CaAl₂O₄:Eu²⁺,Nd³⁺ phosphors by co-doping Gd³⁺. *J. Rare Earths* **2021**, *39*, 930–937. [[CrossRef](#)]
- Chiatti, C.; Fabiani, C.; Pisello, A. Long persistent luminescence: A road map toward promising future developments in energy and environmental science. *Ann. Rev. Mater. Res.* **2021**, *51*, 409–433. [[CrossRef](#)]
- Li, Y.; Gecevicius, M.; Qiu, J. Long persistent phosphors—From fundamentals to applications. *Chem. Soc. Rev.* **2016**, *45*, 2090–2136. [[CrossRef](#)]
- Hai, O.; Ren, Q.; Wu, X.; Zhang, Q.; Zhang, Z.; Zhang, Z. Insights into the element gradient in the grain and luminescence mechanism of the long afterglow material Sr₂MgSi₂O₇:Eu²⁺,Dy³⁺. *J. Alloy. Compd.* **2019**, *779*, 892–899. [[CrossRef](#)]
- Guo, C.; Tang, Q.; Zhang, C.; Huang, D.; Su, Q. Thermoluminescent properties of Eu²⁺ and RE³⁺ co-doped phosphors CaGa₂S₄:Eu²⁺,RE³⁺ (RE = Ln, excluding Pm, Eu and Lu). *J. Lumines.* **2007**, *126*, 333–338. [[CrossRef](#)]
- Cheng, S.; Xu, X.; Han, J.; Qiu, J.; Zhang, B. Design, synthesis and characterization of a novel orange-yellow long-lasting phosphor: Li₂SrSiO₄:Eu²⁺,Dy³⁺. *Powder Technol.* **2015**, *276*, 129–133. [[CrossRef](#)]
- Xu, X.; Yu, X.; Zhou, D.; Qiu, J. Effect of retrapping on the persistent luminescence in strontium silicate orange-yellow phosphor. *J. Solid State Chem.* **2013**, *206*, 66–68. [[CrossRef](#)]
- Zhang, M.; Li, F.; Jiang, S.; Lin, Y.; Chen, F.; Zhao, X.; Shen, Y. CaAl₂O₄:Eu²⁺,Nd³⁺ anti-corrosive coating and its afterglow-Catalytic process. *Opt. Mater.* **2021**, *116*, 111049. [[CrossRef](#)]
- Shi, X.; Dou, R.; Ma, T.; Liu, W.; Lu, X.; Shea, K.; Song, Y.; Jiang, L. Bioinspired lotus-like self-illuminous coating. *ACS Appl. Mater. Interfaces* **2015**, *7*, 18424–18428. [[CrossRef](#)]

30. Wan, M.; Jiang, X.; Nie, J.; Cao, Q.; Zheng, W.; Dong, X.; Fan, Z.; Zhou, W. Phosphor powders-incorporated polylactic acid polymeric composite used as 3D printing filaments with green luminescence properties. *J. Appl. Polym. Sci.* **2020**, *137*, 48644. [[CrossRef](#)]
31. Perez, C.; Collazo, A.; Izquierdo, M.; Merino, P.; Novoa, X. Characterisation of the barrier properties of different paint systems: Part II. non-ideal diffusion and water uptake kinetics. *Prog. Org. Coat.* **1999**, *37*, 169–177. [[CrossRef](#)]
32. Perez, C.; Collazo, A.; Izquierdo, M.; Merino, P.; Novoa, X. Characterisation of the barrier properties of different paint systems: Part I. experimental set-up and ideal Fickian diffusion. *Prog. Org. Coat.* **1999**, *36*, 102–108. [[CrossRef](#)]
33. Zhang, J.; Hu, J.; Zhang, J.; Cao, C. Studies of impedance models and water transport behaviors of polypropylene coated metals in NaCl solution. *Prog. Org. Coat.* **2004**, *49*, 293–301. [[CrossRef](#)]
34. Zhang, J.; Hu, J.; Zhang, J.; Cao, C. Studies of water transport behavior and impedance models of epoxy-coated metals in NaCl solution by EIS. *Prog. Org. Coat.* **2004**, *51*, 145–151. [[CrossRef](#)]

Disclaimer/Publisher's Note: The statements, opinions and data contained in all publications are solely those of the individual author(s) and contributor(s) and not of MDPI and/or the editor(s). MDPI and/or the editor(s) disclaim responsibility for any injury to people or property resulting from any ideas, methods, instructions or products referred to in the content.